Chapter 4

Capturing slow positrons

Slow positrons emitted from the moderator travel back through the bottom entrance tube, following the strong magnetic field lines, and re-enter the trap through the small off-axis aperture in the bottom endcap electrode (see Fig. 2.10). However, they do not *remain* trapped unless they dissipate some energy while inside the trap volume. This chapter explains the details of how positrons lose sufficient energy to be captured in the Penning trap, and how four important bias voltages (the voltage applied to the ring electrode V_{ring}, the voltage applied to the compensation electrodes V_{comp}, the voltage applied to the moderator V_{mod}, and the voltage applied to the entrance tube V_{tube}) directly affect the loading rate R_L.

4.1 Penning trap dynamics

The dynamics of a charged particle (*e.g.* a positron) in a Penning trap are well understood, and are reviewed briefly here. (For a detailed review, see Ref. [22].) The equations in this chapter make use of the fact that the moderated positrons are no longer moving at relativistic energies.

A positron with mass m and charge e in a uniform magnetic field $\mathbf{B}$ moves circularly in the familiar cyclotron motion with a frequency given (in S.I. units)

by

$$2\pi\nu_c = \omega_c = \frac{eB}{m} \tag{4.1}$$

and a radius of

$$r_c = \frac{\sqrt{2E_c m}}{eB}, \tag{4.2}$$

where E_c is the energy in the cyclotron motion. The positron's cyclotron energy comes into thermal equilibrium with the walls of the trap at 4 K by synchrotron radiation damping. The Larmor formula (for example, see Ref. [41]) gives the damping rate for cyclotron motion as

$$\gamma_c = \frac{4r_0\omega_c^2}{3c} \tag{4.3}$$

where $r_0 \simeq 2.8 \times 10^{-13}$ cm is the classical electron radius and c is the speed of light. In 5.9 Tesla the cyclotron frequency $\nu_c \simeq 165$ GHz and $\gamma_c^{-1} \simeq 8 \times 10^{-2}$ sec. Thus, the positron's cyclotron energy after leaving the moderator equilibrates to 4 K in just a few seconds.

The positron's "axial" motion (parallel to the magnetic field lines) is governed by the electrostatic potential produced by the Penning trap electrodes. Figure 4.1 shows an idealized picture of the trap electrodes, along with the electric and magnetic field lines. The endcap and ring electrodes are machined along hyperbola of revolution

$$z^2 = z_0^2 + \rho^2/2 \tag{4.4}$$

and

$$\rho^2 = \rho_0^2 + 2z^2 \tag{4.5}$$

respectively, where ρ_0 and z_0 are the minimum radial and axial distances from the center of the trap to the electrodes. This configuration produces a nearly uniform quadrupole electric potential of the form

$$V(\rho, z) = V_0 \frac{z^2 - \rho^2/2}{2d^2} \tag{4.6}$$

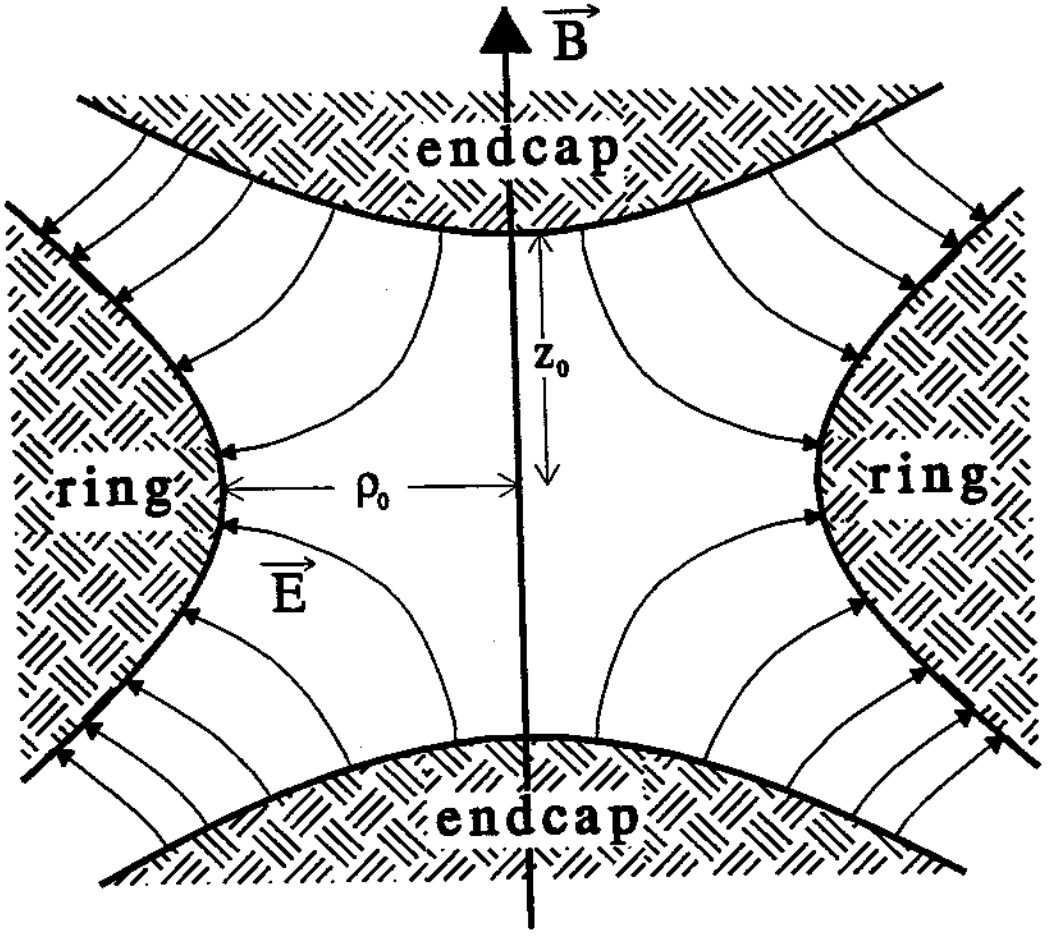

Figure 4.1: Electric and magnetic fields inside a Penning trap.

where V_0 is the voltage applied between the ring and endcaps, and the characteristic trap dimension d is defined by

$$2d^2 = z_0^2 + \rho_0^2/2. \tag{4.7}$$

In practice, machining uncertainties and the truncation of the electrodes cause the electrostatic potential to depart slightly from a pure quadrupole. The voltage applied to the compensation electrodes V_{comp} (see Fig. 2.10) allows us to adjust the electric potential to more closely resemble a pure quadrupole [42], a procedure which is often necessary when performing precision measurements on small clouds

of trapped particles. The trap used in this experiment has $\rho_0 = 0.168$ inches and $z_0 = 0.144$ inches. This ratio of ρ_0/z_0 was chosen to "orthogonalize" the trap electrodes [26,43]. In an "orthogonalized" Penning trap, adjustments in $V_{\rm comp}$ cause little or no shift in ν_z, the frequency of the particle's axial motion, for particles near the center of the trap.

The motional coupling between a positron's cyclotron and axial motion is inconsequential in these traps. Axial motion in the quadrupole electrostatic potential is simple harmonic motion with frequency given by

$$\omega_z^2 = \frac{eV_0}{md^2}. \tag{4.8}$$

The potential between the endcap and ring electrodes is typically $V_0 \simeq 12$ Volts, which gives an axial frequency $\nu_z \approx 69$ MHz. The radiative damping time is too long to be of consequence, so the axial motion is undamped unless it is coupled to a resistive circuit, as described in Section 4.3 and Section 5.1.

The third motion in a Penning trap is typically referred to as "magnetron" motion, and it is caused by the combined magnetic field $\mathbf{B}$ and the radial part of the quadrupole electric field, $\mathbf{E_{rad}}$. The details of the motion are derived elsewhere (see Ref. [22]). Magnetron motion can essentially be thought of as an $\mathbf{E} \times \mathbf{B}$ drift with constant velocity $\mathbf{v} = c\mathbf{E} \times \mathbf{B}/B^2$. Since $|\mathbf{E_{rad}}|$ is proportional to ρ, the magnetron drift has a constant frequency

$$\nu_m = \frac{\nu_z^2}{2\nu_c} \tag{4.9}$$

for all ρ. Assuming $\nu_c = 165$ GHz and $\nu_z = 69$ MHz gives $\nu_m = 14.4$ kHz. The magnetron motion is energetically unstable; that is, as the positron loses magnetron energy, its radius of orbit ρ_{mag} increases. However, the radiative damping time is extremely long ($\gamma_m^{-1} \simeq 3 \times 10^{14}$ sec) and ρ_{mag} can be reduced by applying appropriate radio frequency fields (Section 5.3).

The three motions are pictured in Fig. 4.2. The motions are separable in an ideal quadrupole potential aligned with a uniform magnetic field. Even in a not-

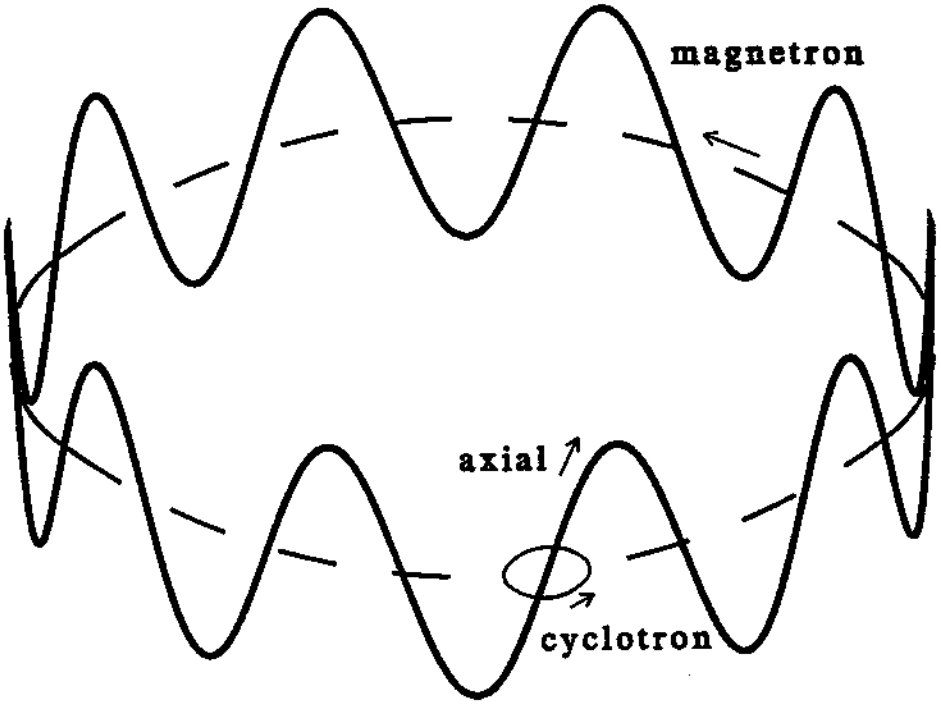

Figure 4.2: Motions of a positron in a Penning trap. The dashed circle is the slow magnetron motion. The solid line shows the axial motion superimposed. The cyclotron motion is much faster with typically a much smaller radius of motion.

quite-ideal trap such as this, the motions can be treated independently for all our calculations.

4.2 Electrostatic potentials in the entrance tubes

The shape of the electrostatic potential in the endcap's off-axis aperture is important for calculating the expected positron loading rate (Section 4.4). A close-up of the area around the off-axis aperture in the bottom endcap is shown in Fig. 4.3. The hole in the endcap has a radius of $r_h = 0.5$ mm and is centered $\rho_h = 0.140$ inches from the central symmetry axis of the trap. The copper entrance

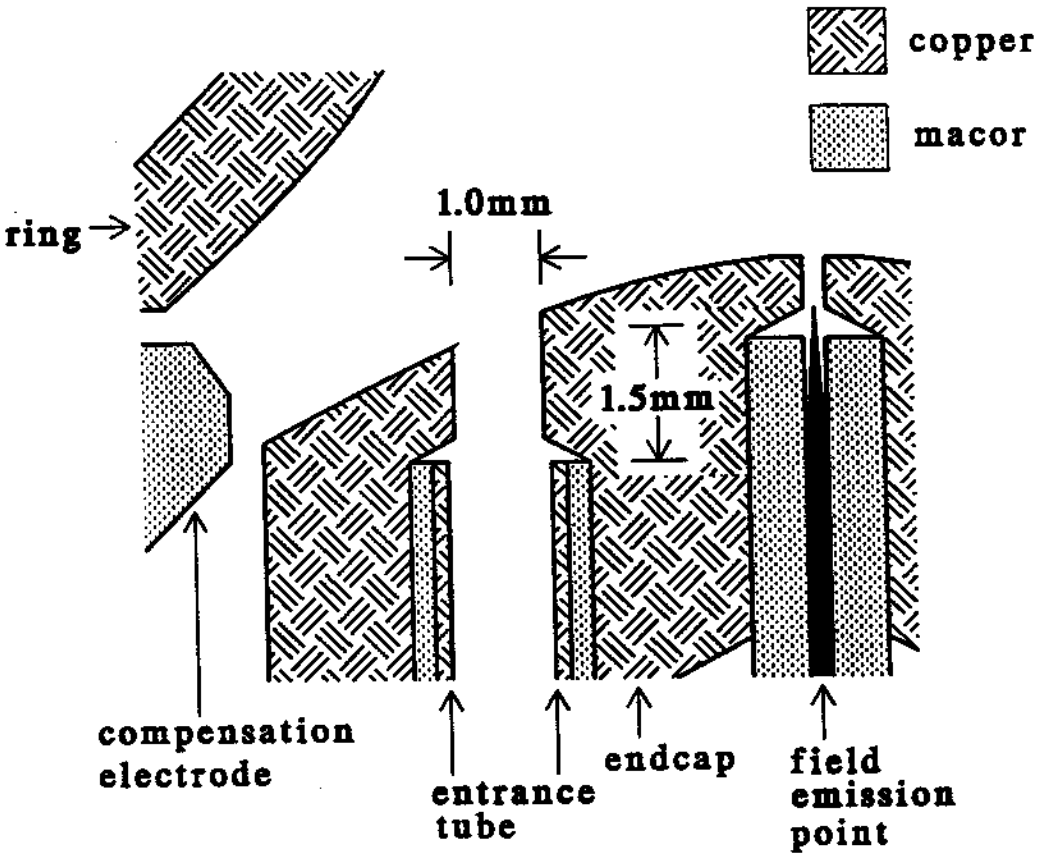

Figure 4.3: The off-axis aperture and entrance tube in the bottom endcap electrode.

tube has a radius $r_{\text{tube}} = 0.7$ mm, and is designed to terminate at a distance of $z'_{\text{tube}} = 1.5$ mm from the point where the center of the entrance aperture intersects with the hyperbolic surface defined by the endcap electrode. (Throughout this chapter, z signifies the (axial) distance from the center of the Penning trap and z' signifies the (axial) distance from the intersection point of the tube's central axial with the bottom endcap electrode surface.)

For positron trapping, the endcaps are grounded, $V_{\text{ring}} \simeq -12$ Volts, and a large negative potential is applied to the bottom entrance tube ($V_{\text{tube}} \simeq -100$ Volts).

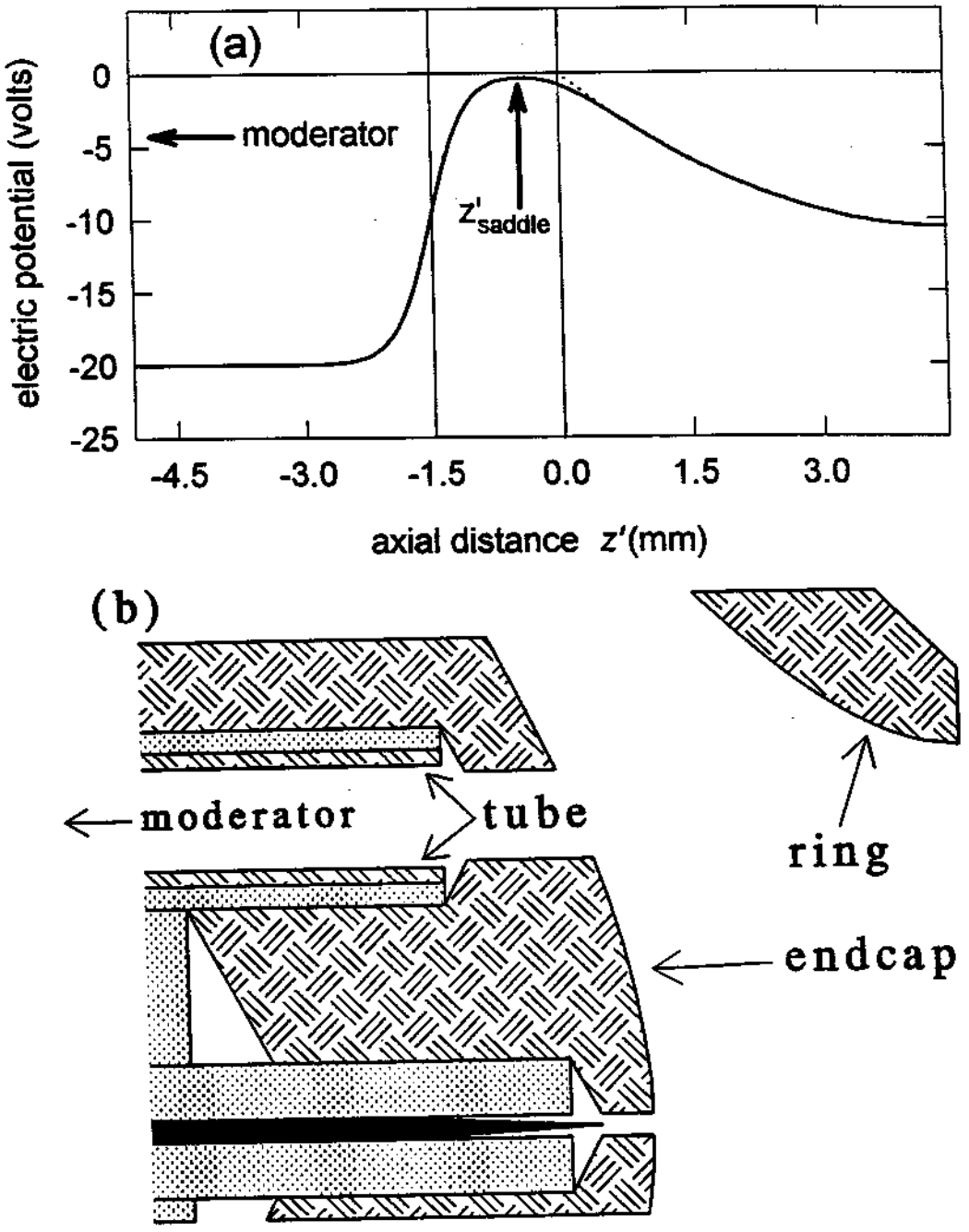

Figure 4.4: (a) Electric potential along the central axis of the loading tube. In this case, $V_{\text{tube}} = -20$ V and $V_{\text{ring}} = -12$ V with the endcaps grounded. The electric potential inside the trap volume ($z' > 0$) is essentially quadratic (dotted line) except in the region near the entrance hole. (b) Corresponding electrode surfaces. The end of the loading tube is located $z'_{\text{tube}} = 1.5$ mm from the hyperbolic surface of the endcap electrode at $\rho = \rho_h$.

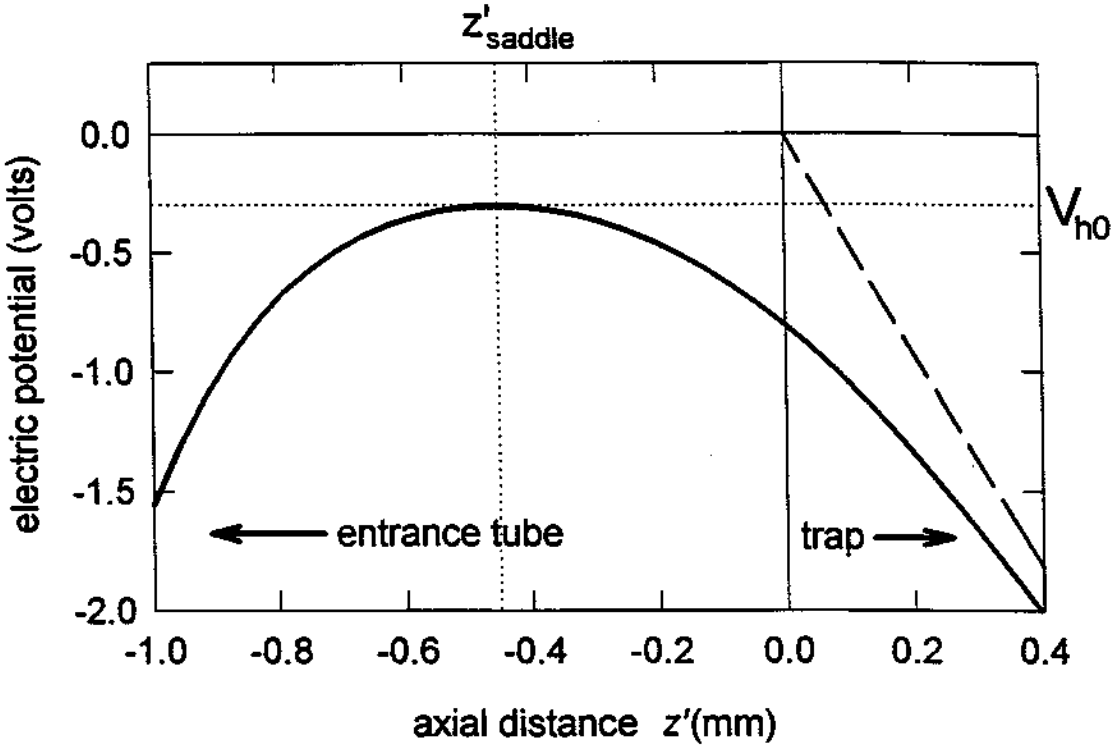

Figure 4.5: Close-up view of electric potential (dark line), as calculated by relaxation technique, along the central axis of the loading tube in the region of the saddle point. V_{h0} and $z'_{\mathbf{saddle}}$ are shown. The dashed line shows a pure quadrupole potential inside the trap ($z' > 0$).

We calculated the electrostatic potential in the region near the entrance aperture in the bottom endcap in two different ways which gave nearly identical results: (1) using a relaxation technique to solve Laplace's equation numerically; (2) solving analytically in three separate regions (inside the trap volume where $z' > 0$. inside the loading tube volume where $z' < -1.5$ mm, and between the tube and trap entrance where -1.5 mm $\leq z' \leq 0$) and matching boundary conditions. The results of these calculations are shown in Figures 4.4 – 4.6. Within the 1.5 mm region *between* the entrance tube and the trap, where the walls of the entrance hole

are grounded, the electric potential $V_h(r, z')$ is best described by a saddle point of the form [1,9]

$$V_h(r, z') = V_{h0}\left(\frac{r_h^2 - r^2 + 2(z' - z'_{\text{saddle}})^2}{r_h^2}\right) \tag{4.10}$$

where $r_h = 0.5$ mm is the radius of the hole, r is the radial distance from the tube's center axis, z'_{saddle} is the (axial) location of the saddle point, and V_{h0} is the potential at the saddle point. Note that $V_{h0} < 0$. The exact values of V_{h0} and z'_{saddle} are given by the calculations and depend upon V_{ring}, V_{tube}, r_{tube}, z'_{tube}, and the electrode geometry. Figure 4.5 shows a close-up of the electrostatic potential along the central axis of the loading tube in the region of the saddle point for the conditions of Fig. 4.4. (The potential departs somewhat from the form of Eq. 4.10 for $z' \neq z'_{\text{saddle}}$ and $r \approx r_h$, but this is not important for our calculations.)

Slow positrons traveling from the moderator (from the left in Fig. 4.4) experience a potential hill at $z' = z'_{\text{saddle}}$. The maximum value of the potential they experience is between V_{h0} and 0, depending upon their radial location r in the tube. Figure 4.6 shows a radial cross-section of $V_h(r, z')$ at $z' = z'_{\text{saddle}}$.

4.3 Damping the axial motion

Once positrons have traveled past the saddle potential and entered the trap, their axial motion can be damped. A positron's axial motion inside the trap induces image charges in the endcap electrodes which oscillate at ν_z. The ring electrode, compensation electrodes, and bottom endcap electrode are all shorted to ground at ν_z through capacitors. The upper endcap, however, is connected to ground through an inductor L which also has a small series loss resistance. On resonance for the LRC circuit, this resistance can be represented as a large parallel resistance R, as shown in Fig. 4.7. The endcap electrode itself contributes to the total capacitance of the circuit. The positron's axial motion causes an oscillating current I to flow

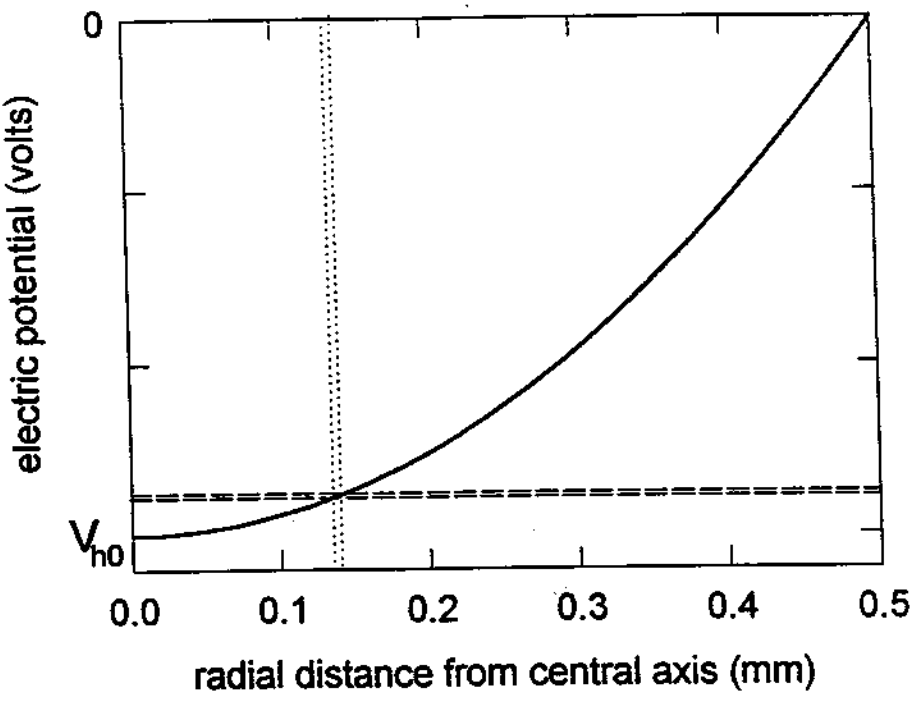

Figure 4.6: The electric potential $V_h(r, z' = z'_{\text{saddle}})$ near the saddle point, as calculated by numerical relaxation (solid curve), is essentially a quadratic function of r. The central axis of the entrance hole corresponds to $r = 0$ and the hole radius is $r_h = 0.5$ mm. The dotted lines are a distance δ_{mag} apart, showing the distance the positron drifts radially during its first axial orbit in the trap. The dashed lines show the corresponding "energy window," which determines the fraction of positrons which "survive" their first axial orbit and remain trapped for a complete magnetron orbit.

through L and R. When V_{ring} and V_{comp} are adjusted so that

$$\omega_z = \omega_{LC} \equiv \sqrt{1/LC}, \tag{4.11}$$

the axial motion is damped at a rate given by [44,45]

$$\gamma_z = \left(\frac{e\kappa}{2z_0}\right)^2 \frac{R}{m}, \tag{4.12}$$

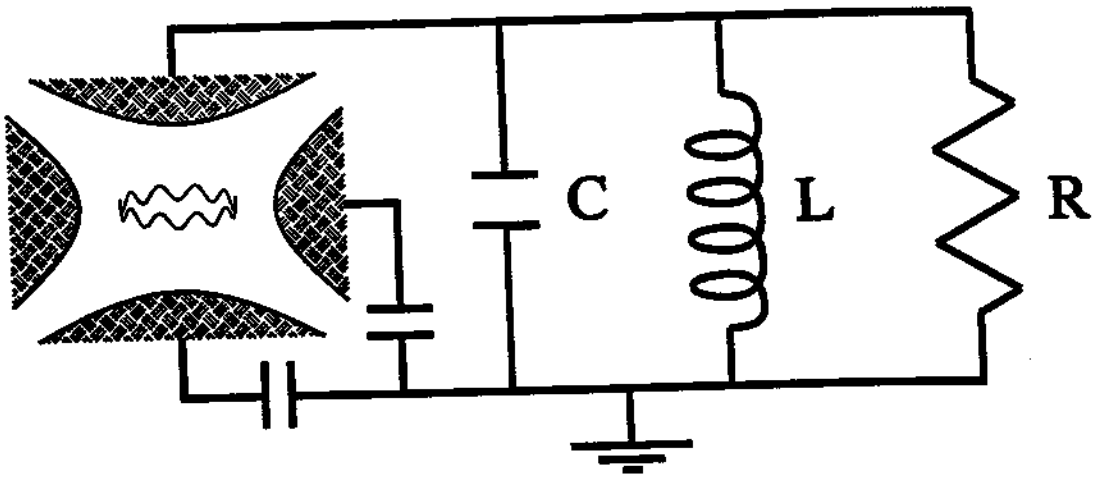

Figure 4.7: Idealization of the circuit connected to the upper endcap. The bottom endcap and ring electrode are shorted to ground at ω_{LC} through large capacitors. The positron's motion induces oscillating current in the resistor, where the energy is dissipated.

where κ is a dimensionless constant of order unity which depends upon the geometry of the trap electrodes. For this trap, $\kappa \simeq 0.8$ has been calculated [26]. We can rewrite Eq. 4.12 as

$$\gamma_z = \left(\frac{\kappa^2 \pi r_0 c}{z_0^2}\right) \frac{R}{\Omega_0} \tag{4.13}$$

where $r_0 = 2.8 \times 10^{-13}$ cm as before and

$$\Omega_0 = \frac{1}{\epsilon_0 c} \simeq 377\,\Omega \tag{4.14}$$

is the familiar "impedance of free space" [22].

A useful number when considering the damping circuit is its quality factor

$$Q = \frac{R}{\omega_{LC} L}. \tag{4.15}$$

The damping constant for a positron's axial motion γ_z scales linearly with Q. In this experiment we used an inductor with $L \simeq 0.27\mu$H. During most of the measurements reported here, $Q \simeq 1000$, with some data taken at $Q \simeq 750$. A quality

factor of 1000 yields $\gamma_z/2\pi \simeq 6.3$ Hz. As we will see in Section 5.4, both γ_z and Q can be measured directly.

We can adjust $V_{\rm mod}$ so that the lowest-energy positrons in the energy spread ΔE have just enough energy to get over the saddle point, so that positrons enter the trap with a range of energies (kinetic plus potential) between V_{h0} and $V_{h0} + \Delta E$. Recall that $V_{h0} < 0$ and that the endcaps are grounded; thus, the moderated positrons do not have sufficient energy to hit the endcaps or escape out the (grounded) upper entrance tube. We also assume that $V_{\rm ring}$ and $V_{\rm comp}$ are adjusted so that the positron's axial motion is resonant with the damping circuit ($\nu_z = \nu_{LC}$).

During the positron's *first* axial orbit in the trap, before returning to the bottom entrance aperture, it loses energy to the damping circuit equal to

$$\delta E_1 = eV_{\rho_h}\frac{\gamma_z}{\nu_z}, \tag{4.16}$$

where V_{ρ_h} is the depth of the axial well at $\rho = \rho_h$. Using Eq. 4.4 and 4.6 we see that $V_{\rho_h} = 0.88V_0$ for this trap. Using the typical values of $V_0 = 12$ Volts, $\nu_z = 69$ MHz, and $\gamma_z/2\pi = 6$ Hz we get $\delta E_1 = 6\,\mu$eV. The fraction of positrons trapped by this mechanism is only $\delta E_1/\Delta E$, which is too small to be significant.

During their first axial orbit, however, positrons also drift laterally in their magnetron orbit [1] a distance

$$\delta_{\rm mag} = 2\pi\rho_{mag}\left(\frac{\nu_m}{\nu_z}\right) \simeq 5\,\mu{\rm m}, \tag{4.17}$$

where $\rho_{mag} = \rho_h = 0.14$ inches is the radius of the magnetron orbit. If $\delta_{\rm mag}$ were larger than the hole radius r_h, all of these positrons would return to the bottom endcap after their first axial orbit sufficiently far from the entrance hole that they would be unable to escape. Because $\delta_{\rm mag} < r_h$, most positrons *do* escape back down the bottom entrance tube after their first axial orbit, annihilating at the moderator; however, a fraction of positrons are captured because of the shape of the electrostatic potential near the saddle point. Recall from Eq. 4.10 and Fig. 4.6

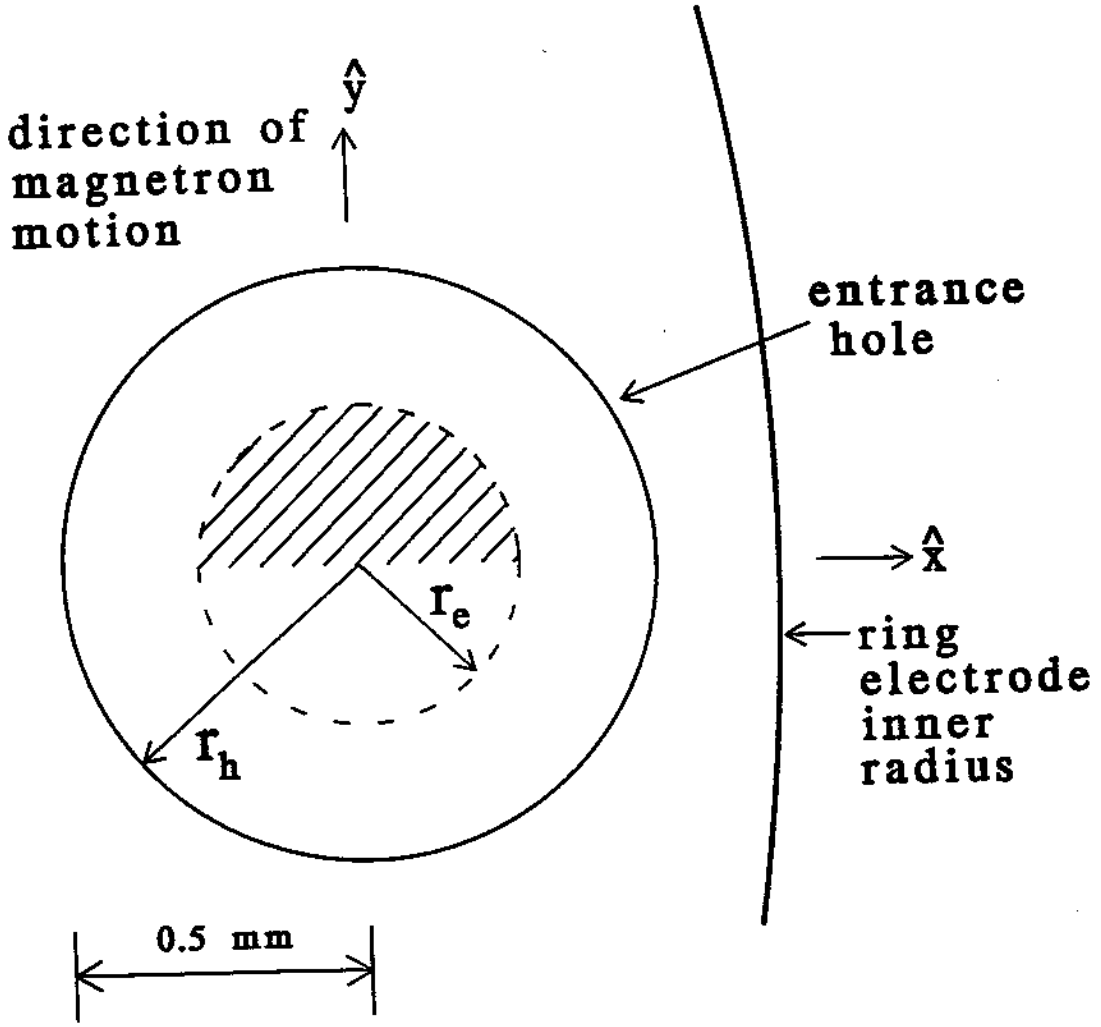

Figure 4.8: Cross-section of the off-axis entrance hole in the bottom endcap showing the active area (shaded region) over which positrons can "survive" their first axial orbit due to magnetron drift and remain in the trap. Note that the positron beam radius is shrunk from $r_h = 0.5$ mm to $r_e \simeq 0.27$ mm due to the average cyclotron radius of the unmoderated positrons, as described in Chapter 2.

that the saddle point of the electric potential is along the entrance tube's central axis. Therefore, if the positron's magnetron drift carries it *away* from the entrance tube's central axis, as shown in Fig. 4.8, the positron essentially "climbs a potential hill." Positrons which fall inside of a narrow energy window, pictured in Fig. 4.6, have insufficient energy to overcome this potential barrier and therefore remain

in the trap after their first axial orbit, for at least one complete magnetron orbit. The fraction of positrons so captured is calculated in Section 4.4. During this first magnetron orbit in the trap the positrons lose axial energy to the damping circuit of

$$\delta E = eV_{\rho_h}\frac{\gamma_z}{\nu_m} \simeq 28\,\mathrm{meV}. \tag{4.18}$$

This is now a significant fraction of ΔE.

4.4 Calculating the expected loading rate

Positron loading into the trap is understood in two nearly independent steps. First, we calculate the fraction of positrons which remain in the trap after their first axial orbit due to magnetron drift. Second, we calculate the total fraction which dissipate sufficient energy to remain in the trap when they return to the entrance tube after their first magnetron orbit.

Consider the x-y plane of the entrance tube at $z' = z'_{\mathrm{saddle}}$. We can rewrite Eq. 4.10 as

$$V_h(x, y, z' = z'_{\mathrm{saddle}}) = V_{h0}\left(\frac{r_h^2 - x^2 - y^2}{r_h^2}\right) \tag{4.19}$$

where (x, y) are defined relative to the entrance hole's central axis and $x^2 + y^2 \leq r_h^2$. Positrons enter the trap with a range of possible (x_i, y_i) such that $x_i^2 + y_i^2 \leq r_e^2$. (Recall from Chapter 2 that r_e, the effective radius of the positron beam when it hits the moderator, is less than r_h due to the cyclotron radius of the unmoderated positrons.) To simplify the following calculations, we assume that positrons enter the trap uniformly over an active area πr_e^2. We also make the simplifying assumption that the positron energies are distributed uniformly over ΔE. which is good for broad energy distributions ($\Delta E > \delta E$).

We define ϵ as the fraction of slow (moderated) positrons which are permanently trapped. A positron entering the trap at $(x_i, y_i, z'_{\mathrm{saddle}})$ magnetron drifts

in its first axial orbit and return to the position $(x_i, y_i + \delta_{\rm mag}, z'_{\rm saddle})$, where we have arbitrarily chosen the entrance tube to be in the $\hat{x}$ direction from the trap's central symmetry axis so that the initial magnetron drift is in the $\hat{y}$ direction. For each (x, y) the fraction of positrons which remain trapped after their first axial orbit is the difference in the potential energy of the positron before and after the first axial orbit, divided by the initial energy spread [9],

$$\epsilon_{init}(y) = \frac{eV_h(x, y+\delta_{\rm mag}) - eV_h(x,y)}{\Delta E} \approx \frac{2e|V_{h0}|\,\delta_{\rm mag} y}{r_h^2 \Delta E} \tag{4.20}$$

for $y > 0$, with no positrons trapped in the $y < 0$ region. We can integrate over $(x^2 + y^2) \leq r_e^2$ to obtain

$$\epsilon_{init} = \frac{4 r_e \delta_{\rm mag} e|V_{h0}|}{3\pi r_h^2 \Delta E}. \tag{4.21}$$

A positron which enters the trap at $(x_i, y_i, z' = z'_{\rm saddle})$ and remains in the trap after its first axial orbit will, after one magnetron orbit, return to the entrance tube having lost $\delta E \approx 28$ meV of axial energy to the damping circuit. When it reaches the position $(x_i, y = 0, z' = z'_{\rm saddle})$ it encounters a minimum in the electric potential along its trajectory. If the positron's initial kinetic-plus-potential energy upon entering the trap was δE *greater* than its potential energy at $(x_i, y = 0, z' = z'_{\rm saddle})$, it escapes down the entrance tube and is lost. Conversely, if the positron's initial kinetic-plus-potential energy was *less* than δE plus its potential energy at $(x_i, y = 0, z' = z'_{\rm saddle})$, it remains trapped. (Since the range of *kinetic* energies which are initially trapped is small—that is, $\Delta E \cdot \epsilon_{init}(y) \ll e|V_{h0}|$ in general—we can restrict our attention to the potential energies involved.) This restricts the "active area" for positron trapping to $0 \leq y_i \leq y_D$, where

$$y_D^2 = r_h^2 \left(\frac{\delta E}{|V_{h0}|} \right). \tag{4.22}$$

Positrons which enter the trap with $y_i > y_D$ do *not* remain in the trap after their first magnetron orbit because

$$V_h(x_i, y = y_i, z' = z'_{\rm saddle}) - V_h(x_i, y = 0, z' = z'_{\rm saddle}) > \delta E. \tag{4.23}$$

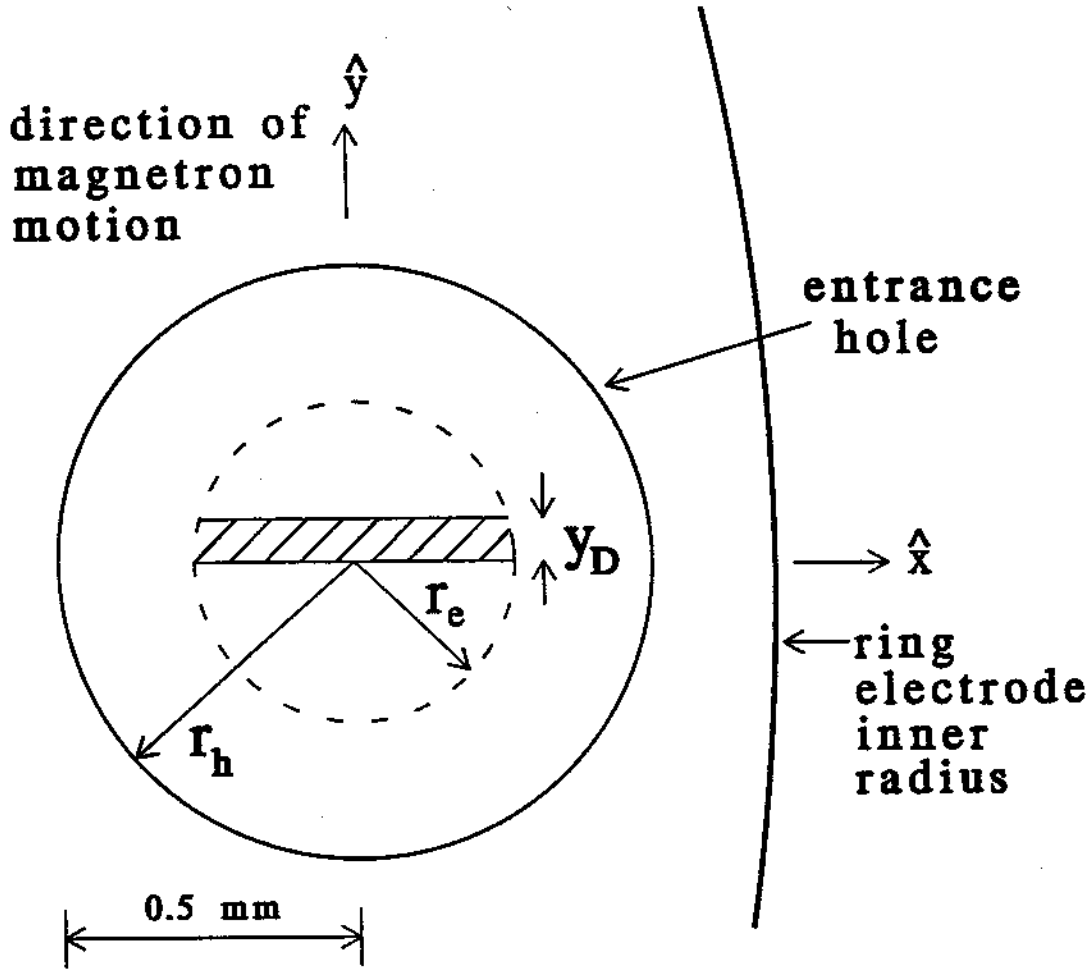

Figure 4.9: Cross-section of the entrance hole showing the active area over which positrons can be *permanently* loaded into the trap. The distance y_D is given by Eq. 4.22.

Figure 4.9 shows the active area over which positrons can enter and remain *permanently* trapped.

Once a positron has "survived" its first magnetron orbit, it continues to lose energy to the damping circuit until it comes into thermal equilibrium (at 4 K). After that, it should remain trapped indefinitely. Other possible mechanisms for positron loss from the trap are discussed in Section 6.2. We expect no loss of

positrons during a normal accumulation cycle.

If we assume that $\delta E < \Delta E$, which is the case for all the damping circuits and moderators we have used to date, we calculate the total trapping efficiency for moderated positrons, ϵ, by integrating Eq. 4.20 over the active trapping window, giving

$$\begin{aligned}
\epsilon &= \frac{4r_e\delta_{\rm mag}e|V_{h0}|}{3\pi r_h^2\Delta E}, && e|V_{h0}|(\tfrac{r_h^2}{r_e^2}) < \delta E < \Delta E; \\
&= \frac{2\delta_{\rm mag}\delta E}{\pi r_e\Delta E}, && \delta E < e|V_{h0}|(\tfrac{r_h^2}{r_e^2}) < \Delta E; \\
&= \frac{2r_h\delta_{\rm mag}\delta E}{\pi r_e^2\Delta E}\sqrt{\frac{\Delta E}{e|V_{h0}|}}, && \delta E < \Delta E < e|V_{h0}|(\tfrac{r_h^2}{r_e^2}).
\end{aligned} \tag{4.24}$$

When $|V_{h0}|$ is small (first condition of Eq. 4.24), $y_D > r_e$ and the active trapping window includes the entire shaded area of Fig. 4.8. For larger $|V_{h0}|$, we obtain the second condition of Eq. 4.24 and the active trapping window is the shaded region of Fig. 4.9. The third condition of Eq. 4.24 holds when

$$V_h(r = r_e, z' = z'_{\rm saddle}) - V_h(r = 0, z' = z'_{\rm saddle}) > \Delta E, \tag{4.25}$$

in which case the "trapping window" shown in Fig. 4.9 covers a region of potential energies larger than ΔE, which reduces the trapping efficiency.

The analysis of Eq. 4.24 is slightly modified when $\Delta E < \delta E$ with the result

$$\begin{aligned}
\epsilon &= \frac{4r_e\delta_{\rm mag}e|V_{h0}|}{3\pi r_h^2\Delta E}, && e|V_{h0}|(\tfrac{r_h^2}{r_e^2}) < \Delta E < \delta E; \\
&= \frac{2r_h\delta_{\rm mag}}{\pi r_e^2}\sqrt{\frac{\Delta E}{e|V_{h0}|}}, && \Delta E < e|V_{h0}|(\tfrac{r_h^2}{r_e^2}).
\end{aligned} \tag{4.26}$$

We can calculate ϵ more accurately by integrating Eq. 4.24 over the distribution of cyclotron radii shown in Fig. 2.11; however, this yields the same result as using $r_e \approx 0.27$ mm.

We can adjust $V_{\rm tube}$ to obtain the second condition of Eq. 4.24, which is optimal. Using $r_e = 0.27$ mm, Eqs. 4.17 and 4.18, and a measured $\Delta E = 230$ meV, we

estimate a capture efficiency $\epsilon \simeq 1.5 \times 10^{-3}$. If we can reduce ΔE to 65 meV, we will obtain $\epsilon \simeq 5 \times 10^{-3}$.

The expected positron loading rate R_L is the product of the (fast) positron flux on the moderator F, the moderator efficiency η, and the slow positron trapping efficiency ϵ (which is itself a function of of the moderated positrons' energy spread ΔE). Combining Eq. 2.6 and the second condition of Eq. 4.24 gives

$$R_L = \eta A \frac{B_t}{B_s}\left[1 - \sqrt{\left(1 - \frac{B_s}{B_t}\right)}\right]\left(\frac{2r_e\delta_{\mathrm{mag}}}{\pi r_s^2}\right)\left(\frac{\delta E}{\Delta E}\right), \tag{4.27}$$

where A is the source activity in positrons per second, and B_s and B_t are the magnetic fields at the source and trap, respectively. If $\eta = 1 \times 10^{-4}$ and $\Delta E = 230$ meV we expect a total loading rate of $R_L \approx$0.5 e^+/s. If $\eta = 1 \times 10^{-3}$ and $\Delta E = 65$ meV we expect $R_L \approx 15$ e^+/s.

There is a complicating factor which could reduce the loading rate from our calculated value. The axial motion damping term δE calculated in Eq. 4.18 and the trapping efficiency ϵ calculated in Eq. 4.24 are valid only when the positron's axial motion is harmonic (or very nearly so) and at a frequency matched to the frequency of the LRC damping circuit ($\nu_z = \nu_{LC}$.) The positron's axial motion should be harmonic (that is, the axial frequency is independent of the amplitude) so long as the electric potential it experiences $V(\rho, z)$ is purely quadrupole. Penning traps of this geometry (shown in Fig. 2.10) are known [26,43] to produce electrostatic potentials which are very nearly quadrupole in the center of the trap ($\rho \approx z \approx 0$). Near the electrode surfaces, however, the potential can depart significantly from the quadrupole form, primarily due to the truncation of the electrodes—although hyperbolically shaped electrodes cause less anharmonicity near the electrode surfaces than other possible geometries (*e.g.* cylindrical). The positron's first axial and magnetron orbits take place very near the edges of the trap ($\rho = \rho_h \approx \rho_0$ and $z_{\mathrm{max}} > z_0$), where any anharmonicities in the potential are the greatest. This decreases coupling between the large-amplitude axial motion and the damping circuit. Therefore, the actual damping term δE and loading rate

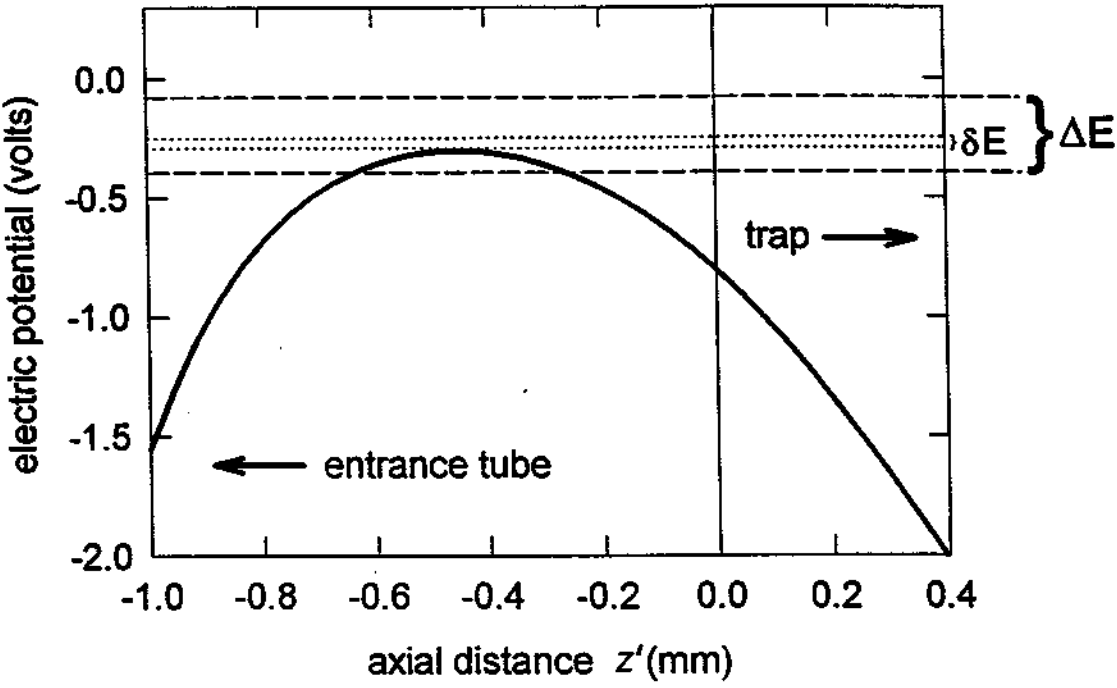

Figure 4.10: Energy window for trapping positrons along the entrance tube's central axis.

R_L may be somewhat lower than what we calculate in Eq. 4.27.

4.5 Measured loading rate

The calculations of previous section allow us to determine how the loading rate R_L should depend upon the four important bias voltages: V_{ring}, V_{comp}, V_{tube}, and V_{mod}. We now compare those expectations with our experimental results.

4.5.1 Loading rate dependence on tube and moderator bias

In order to trap positrons, V_{mod} must be adjusted to nearly cancel the kinetic energy with which positrons leave the moderator, ϕ_+. Ideally, V_{mod} is adjusted so that the spread of positron energies ΔE completely covers the "energy window" over which positrons can be trapped, which is between V_{h0} and $V_{h0} + \delta E$ for positrons entering along the tube's central axis, as shown in Fig. 4.10. When δE and $|eV_{h0}|$ are considerably less than ΔE, measuring the positron loading rate R_L as a function of V_{mod} allows us to sensitively measure the energy distribution of moderated positrons. There are several examples of R_L measured *vs.* V_{mod} in Chapter 3. All of those graphs were taken at a constant V_{tube}.

The loading rate depends upon V_{tube} only insofar as adjusting V_{tube} changes V_{h0}. As Eq. 4.24 shows, for small $|V_{h0}|$ we expect the loading rate R_L to increase linearly with $|V_{h0}|$; for large $|V_{h0}|$ the loading rate R_L should decrease slowly as $|V_{h0}|$ increases. Moreover, we expect that the value of V_{mod} which gives the maximum loading rate will shift with V_{tube} equal to the change in V_{h0}, since the loading rate is maximized when $\phi_+ + eV_{\text{mod}} = eV_{h0}$.

Figure 4.11 shows the measured loading rate *vs.* V_{mod} for nine different values of V_{tube}. As expected, the location of the V_{mod} peak shifts as V_{tube} is varied. By plotting the peak loading rates of Fig. 4.11 *vs.* V_{h0} (Fig. 4.12), we see exactly the dependence which we expect from Eq. 4.24. Note also from Fig. 4.11 that the apparent width of the positron energy distribution ΔE grows for large values of $|V_{h0}|$. This is because positrons are trapped whenever some portion of ΔE overlaps the "energy window" corresponding to the "active trapping window" shown in Fig. 4.9. When this "energy window" is greater than ΔE, we should expect the measured energy distribution to be broadened. We obtain an accurate measurement of ΔE only when $|V_{h0}| < \Delta E$.

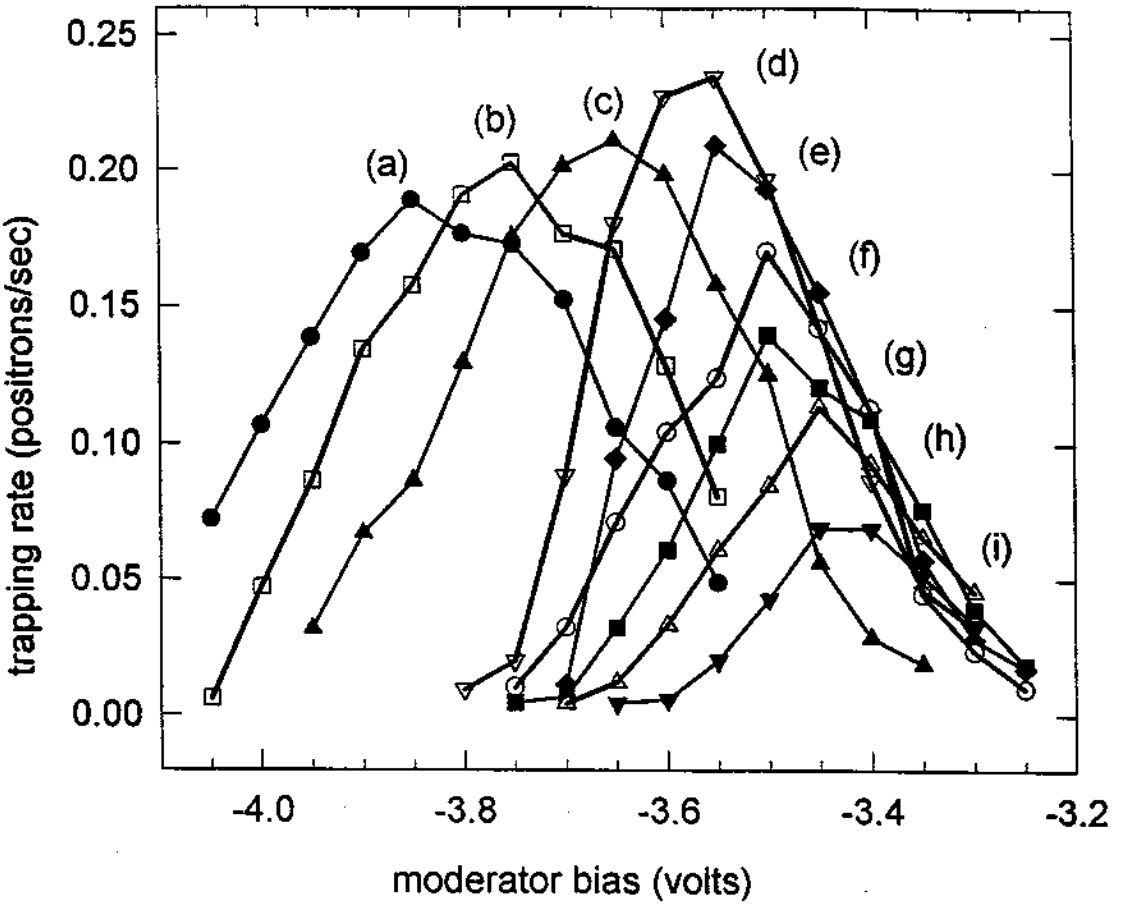

Figure 4.11: Positron trapping rate *vs.* moderator bias (using the moderator which gave the narrowest positron energy spread) for several different loading tube potentials. (a) V_{tube} = –250 Volts; (b) V_{tube} = –200 Volts; (c) V_{tube} = –150 Volts; (d) V_{tube} = –100 Volts; (e) V_{tube} = –60 Volts; (f) V_{tube} = –50 Volts; (g) V_{tube} = –40 Volts; (h) V_{tube} = –30 Volts; (i) V_{tube} = –20 Volts.

4.5.2 Loading rate dependence on ring and compensation bias

Adjusting V_{ring} causes the positron's axial frequency ω_z to shift an amount given by Eq. 4.8. As ω_z shifts away from ω_{LC}, the positron's axial motion is damped less effectively, causing the positron loading rate to decrease. This is demonstrated

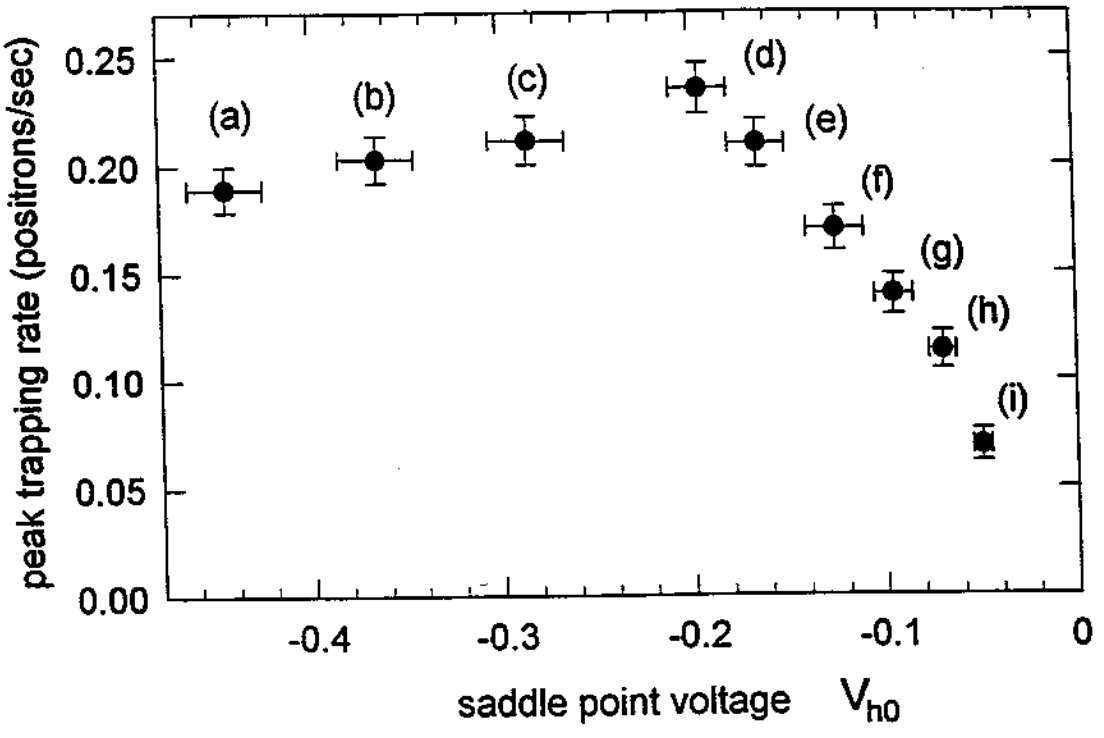

Figure 4.12: Peak trapping rate *vs.* the saddle point potential V_{h0} for the nine different values of V_{tube} shown in the previous figure.

in Fig. 4.13, which shows the measured positron loading rate *vs.* V_{ring} for three fixed values of $V_{\text{comp}}/V_{\text{ring}}$. We also note from Figure 4.13 that the peak loading rates for curves (a) and (c) are smaller than the peak loading rate for curve (b). When V_{comp} is adjusted too far positive or too far negative, the electric potential $V(\rho, z)$ inside the trap becomes increasingly anharmonic, which decreases the loading rate.

Figure 4.13 also shows that the value of V_{ring} which maximizes positron loading changes as V_{comp} is adjusted. This is better illustrated in Fig. 4.14, which shows a three-dimensional plot of loading rate (vertical axis) versus ring and compensation voltage simultaneously. The loading rate is highest along a "ridge" in the V_{ring}—V_{comp} plane. We interpret this ridge to correspond to voltages which

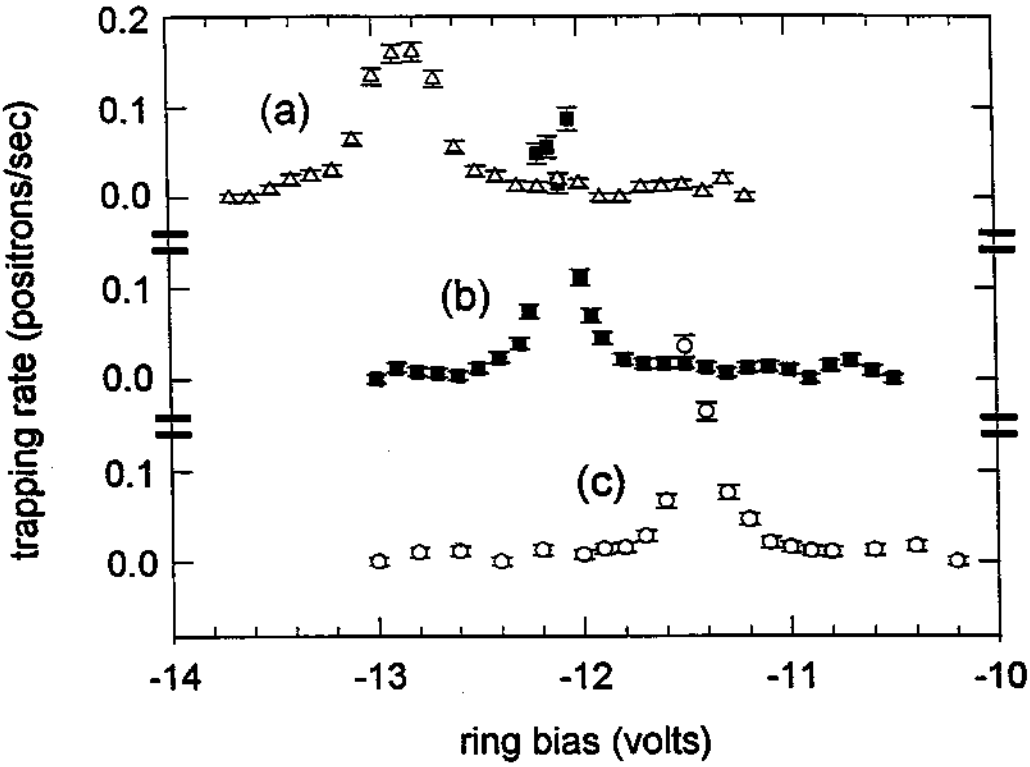

Figure 4.13: Positron trapping rate *vs.* ring bias for three values of $V_{\rm comp}$. (a) $V_{\rm comp}/V_{\rm ring} = -2.5$; (b) $V_{\rm comp}/V_{\rm ring} = +0.5$; (c) $V_{\rm comp}/V_{\rm ring} = +3.5$.

cause $\omega_z = \omega_{LC}$. We see that, as expected, ω_z depends much more strongly on $V_{\rm ring}$ than on $V_{\rm comp}$, and that the height of the ridge falls off somewhat, though not dramatically, for large (negative or positive) values of $V_{\rm comp}/V_{\rm ring}$.

The electric potential inside this hyperbolic Penning trap has been computed using a relaxation technique to solve Laplace's equation numerically [26,43]. This allows us to calculate the actual shape of the electric potential which the positron experiences during its axial orbits at $\rho = \rho_h$, which in turn allows us to compute the expected dependence of ω_z upon $V_{\rm comp}$, as a function of the amplitude of the axial motion. The results are shown in Fig. 4.15. Also shown is our *measured* frequency shift for damping the large-amplitude axial motion of our positrons—

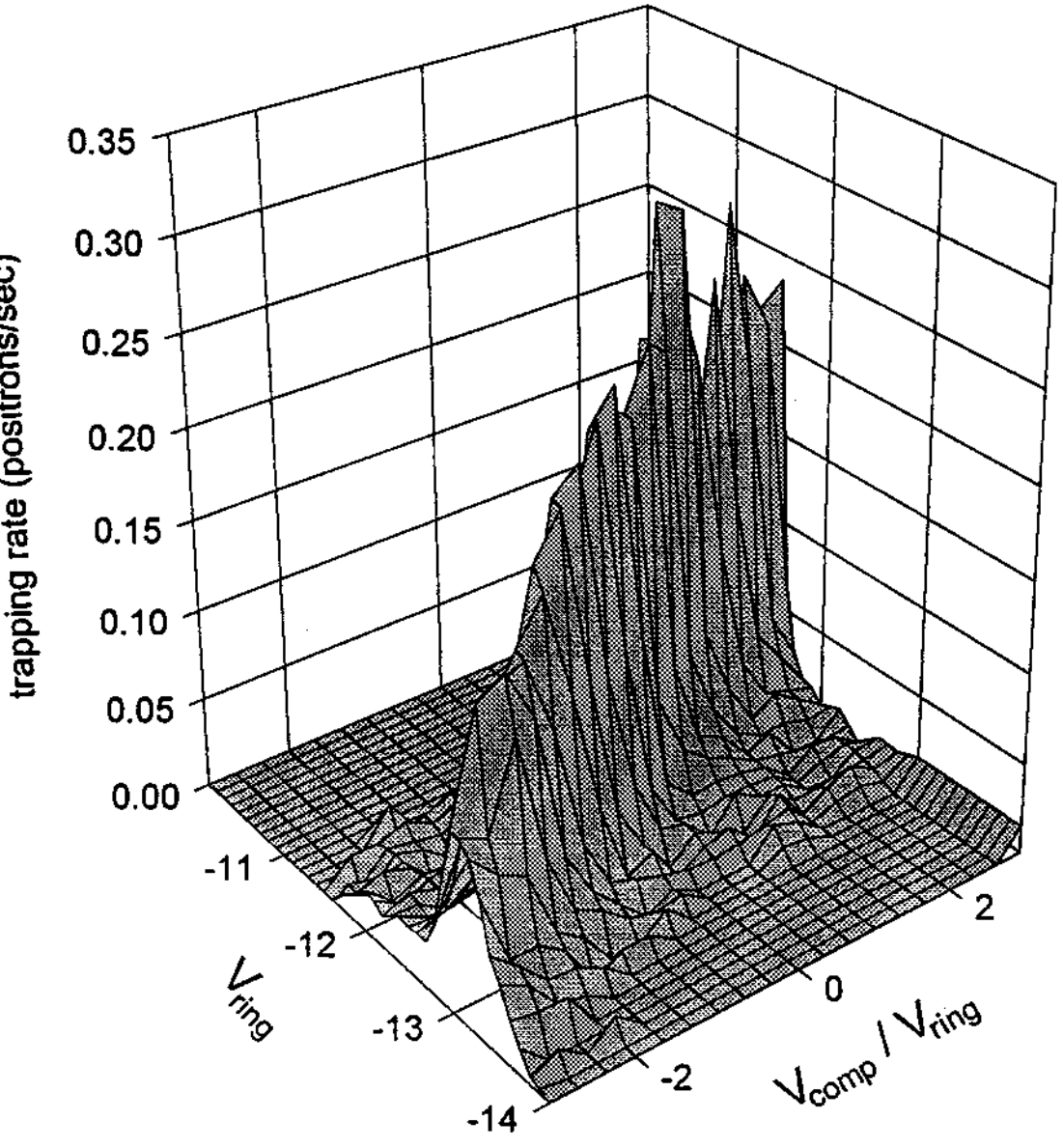

Figure 4.14: Positron trapping rate (vertical axis) *vs.* V_{ring} and the degree of compensation, $V_{\text{comp}}/V_{\text{ring}}$.

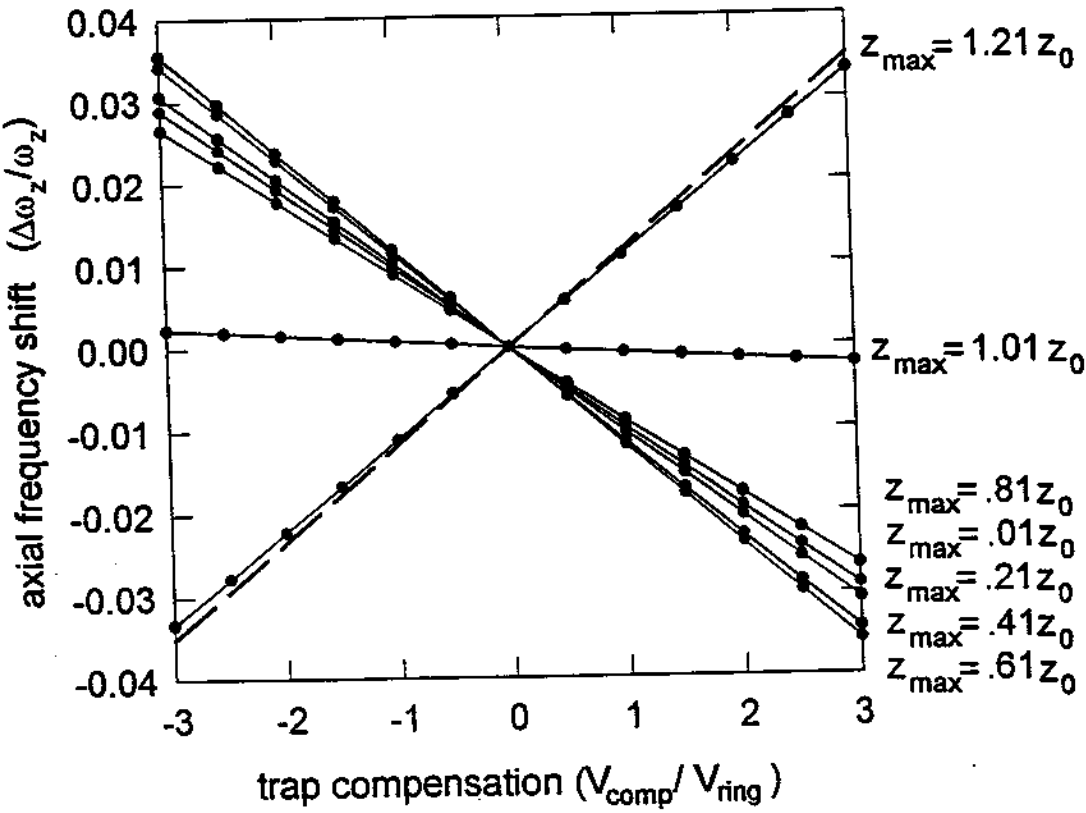

Figure 4.15: Expected shift in the positron axial frequency due to trap compensation, for several values of axial motion amplitude at $\rho = \rho_h$. The points are from computer simulations using the results of the relaxation calculation. During a positron's first magnetron orbit in the trap its axial amplitude is large, with $z_{max} = \sqrt{z_0^2 + \rho_h^2/2} = 1.21\ z_0$. The dashed line corresponds to the measured location of the "ridge" in Fig. 4.14.

which corresponds to the direction of the "ridge" in Fig. 4.14. We see that the measured "ridge" matches our calculated values for large-amplitude axial orbits at $\rho = \rho_h$. The relaxation calculation was performed for a trap without entrance apertures. The excellent agreement between calculation and experiment suggests that the positron's axial frequency is not greatly affected by the apertures during

most of its magnetron orbit.

The slopes of the lines in Fig. 4.15 can be understood qualitatively in the following way: for orbits with a large magnetron radius ($\rho_{mag} = \rho_h \approx \rho_0$) and a small axial amplitude ($z < .8\, z_0$), the compensation electrodes behave more like endcap electrodes to the positrons—that is, they are farther from the positrons in the axial direction than in the radial direction. Since we would expect a positive voltage on the endcap electrodes to *increase* ω_z (and conversely, a negative endcap voltage to decrease ω_z), we would also expect a positive $V_{\rm comp}$ to increase ω_z for small-amplitude orbits. (Recall that $V_{\rm ring} < 0$.) As the axial amplitude becomes large ($z_{\rm max} > z_0$), the positrons spend a large fraction of their orbits *between* the endcap and the compensation electrode. In this region, we would expect the compensation electrodes to behave more like the ring electrode in its effect; and we would expect the axial frequency dependence on $V_{\rm comp}$ to change its sign. These expectations are confirmed by both the simulation and by experimental results.

Figure 4.16 shows the frequency spectrum of the (4 K) thermal noise in the LRC damping circuit when the trap is empty of positrons, which reveals a typical Lorentzian shape with a center frequency of 69.780 MHz and a full width at half-maximum (FWHM) of $\sim$ 90 kHz. According to Eq. 4.8, a shift in the positrons' axial frequency of 90 kHz corresponds to a shift in $V_{\rm ring}$ of 30 mV. (We routinely verify Eq. 4.8 for small-amplitude orbits near the center of the trap, where the electrostatic potential is nearly a pure quadrupole.) Note from Fig. 4.13 that the full width at half maximum of the peak loading rate, as a function of $V_{\rm ring}$, is typically FWHM $\simeq$ 300 mV. This is approximately ten times larger than we would have expected, given a damping circuit quality factor of $Q = 780$ and harmonic axial orbits. This suggests that the large-axial-amplitude, large-magnetron-radius orbits of our positrons when they first enter the trap are somewhat anharmonic, and may also account for the fact that we typically measure a peak loading rate of $R_L \simeq 0.2\ e^+/s$, rather than the rates calculated in Eq. 4.27.

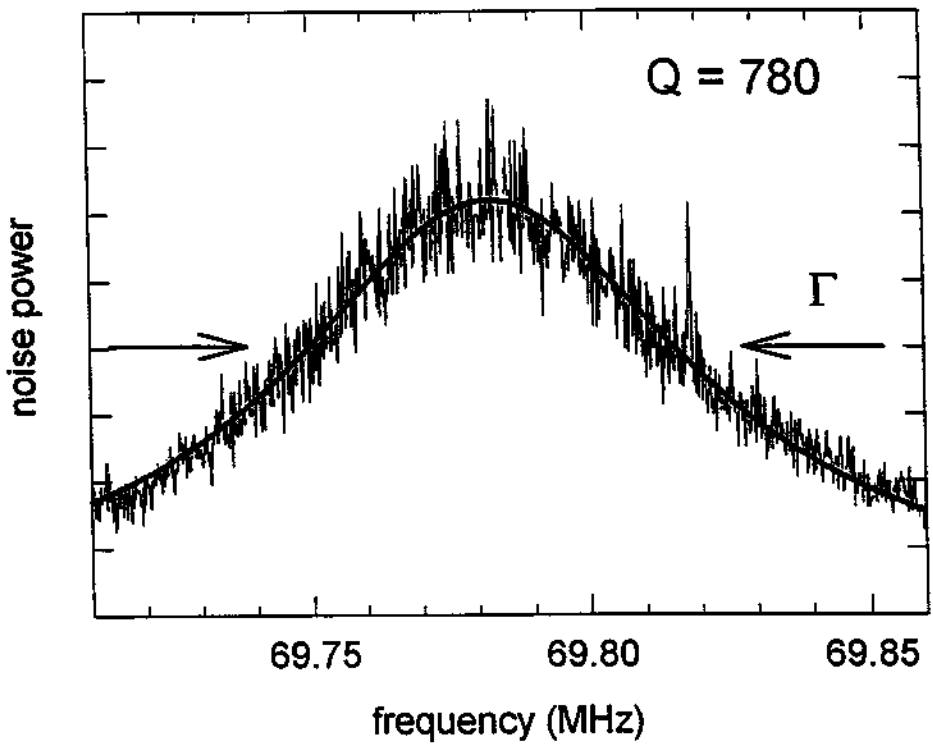

Figure 4.16: Frequency spectrum of the (4 K) thermal noise in the LRC damping circuit when the trap is empty. The darker line is a best-fit Lorentzian; the FWHM of the noise power gives the circuit's quality factor $Q = 780$. The small peak at 69.818 MHz comes from noise external to the apparatus.

4.6 Design changes to increase the loading rate

Having shown that our measured loading rate R_L is the same order of magnitude as our expectations, and that it depends upon the trapping parameters V_{ring}, V_{comp}, V_{mod}, and V_{tube} as predicted, we now consider possible design changes to the trap which could result in an increased loading rate. To facilitate this discussion, we rewrite Eq. 4.27 in terms of the physical parameters of the positrons, the Penning trap, the damping circuit, and the moderator (rather than using calculated terms

such as δE and δ_{mag}) by using Eq. 4.8, 4.12, 4.17, and 4.18, yielding

$$R_L = \frac{\eta A}{\Delta E}\left(\frac{2\pi r_e}{r_s^2}\right)\sqrt{\frac{m}{e^5}}\frac{B_t}{B_s}\left[1-\sqrt{\left(1-\frac{B_s}{B_t}\right)}\right]\left(\frac{\kappa^2\rho_h d}{z_0^2}\right)\sqrt{V_0}R. \tag{4.28}$$

Simply increasing or decreasing the physical size of the Penning trap has no large effect, since the term in parenthesis on the right side of Eq. 4.28 is approximately equal to one ($z_0 \approx \rho_h \approx d$).

The (unmoderated) positron flux on the moderator could be increased by moving the radioactive source closer to the trap (so that $B_s = B_t$) to eliminate "magnetic bouncing" (the term in brackets), while simultaneously increasing the size of the trap's entrance apertures so that $r_e \approx r_s$. This would increase the flux (proportional to r_e^2/r_s^2) by a factor of 28; however, the loading rate would only increase by a factor of 7 because R_L is proportional to the positron flux in the *active trapping window* shown in Fig. 4.9, which scales as r_e/r_s. One possible concern with this modification is that the increased apertures would adversely affect the harmonicity of the trap, causing decreased axial motion damping. This is not a serious problem once the positron's magnetron orbit carries it well away from the apertures (more than two hole radii for most of the orbit) where the effect of the apertures is small. The effective aperture radius r_e could also be increased by increasing the overall magnetic field strength, which would shrink the cyclotron radii of the unmoderated positrons.

Another way to increase the positron flux on the moderator—provided appropriate precautions are taken for the safety of the experimenters—is to increase the source activity A (without increasing its active area πr_s^2). The measurements reported in this thesis were taken when our source activity had decreased to between 10 and 12 mCi. Loading rates could be increased by a factor of 2 by purchasing a new source of the same design at 20 mCi. As noted in Section 2.1, our source self-absorbs an estimated 50% of its positrons due to the thickness of the source material. Therefore, increasing the source activity beyond 20 mCi by further increasing the source material thickness would cause little increase in positron flux.

Other positron-producing radionuclei (*e.g.* ^{58}Co) could produce more positrons over the same active area, but at the expense of a greatly reduced half-life.

If still higher loading rates are desired without further increasing the entrance apertures, it would be possible to place a more intense source (with larger active area) and moderator ***outside*** of the strong magnetic field and focusing the moderated beam onto a remoderator near the trap [9]. A 150 mCi ^{22}Na source such as is used at U.C. San Diego [46] would increase loading rates by a factor of 3 to 15, depending on the efficiencies of the moderator and remoderator.

The positron loading rate is directly proportional to the moderator efficiency η and inversely proportional to ΔE. The narrowest positron energy spread we have so far achieved is $\Delta E \simeq 230$ meV, which is considerably larger than the value $\Delta E \simeq 65$ meV reported in the literature [32,33]. This may be due to the difficulties of moderator preparation in a sealed, cryogenic environment, or due to the quality of the crystal itself. Achieving ΔE = 65 meV would increase our loading rate by a factor of 3.5.

The magnetic field strength does not directly affect ϵ, the capture efficiency for moderated positrons. An increase in B (while keeping V_0 fixed) would cause the the magnetron frequency ω_m to decrease. This would simultaneously cause $\delta_{\mathbf{mag}}$ to decrease and δE to increase proportionately, with no net change in the capture efficiency for $\delta E < \Delta E$.

Increasing V_0 (equal to $|V_{\mathbf{ring}}|$ when the endcaps are grounded) would increase the loading rate, but would also necessitate increasing the resonant frequency of the damping circuit to keep $\omega_{LC} = \omega_z$, which would have some effect on R. The effective parallel resistance R of the damping circuit (at ω_{LC}) is proportional to its quality factor Q,

$$R = \frac{Q}{\omega_{LC} C}. \tag{4.29}$$

The capacitance of the LRC circuit is usually fixed by the size of the endcap electrodes, and Q typically scales with the square root of ω_{LC} for these circuits.

Therefore, the net increase in the positron loading rate effectively scales only as the fourth root of V_0. Increasing the trapping voltages to 1000 Volts (and scaling the LRC circuit appropriately) would give us only a factor of 3 increase in loading rate. Still higher voltages would be impossible without substantially redesigning the apparatus (vacuum feedthroughs, transmission lines, filter capacitors, and the trap electrodes themselves).

It is also possible to increase Q (without changing ω_{LC} or V_0) by modifying the LRC circuit. Quality factors as high as $Q = 1450$ have been achieved on a similar Penning trap at similar frequencies [47]. This would increase our loading rate by a factor of 2, since R_L scales linearly with Q so long as $\delta E < \Delta E$.

It may be possible to improve the harmonicity of the positron's large-axial-amplitude, large-magnetron-radius motion (when it first enters the trap) by adding one or more additional sets of compensation electrodes. We know that the full-width half-maximum of our measured loading rate dependence upon V_{ring} is 10 times larger than expected (from the Q of the damping circuit), and we suspect this is due to anharmonicity in the positron's axial motion (Section 4.5.2). The additional electrodes would provide better control over the shape of the electrostatic potential. It is difficult to know whether this would increase the loading rate (by at most a factor of 10) without performing detailed relaxation calculations of the type done in Refs. [26] and [43].

Finally, it may be possible to increase the positron's magnetron drift distance during its first axial orbit δ_{mag}—without changing the magnetron frequency ω_m—by splitting the *upper* entrance tube. We expect that biasing the (unsplit) upper entrance tube (see Fig. 2.10) should cause little or no change in the loading rate, and this has been verified experimentally. If, however, the upper entrance tube were split into four quadrants, the quadrant of the tube closest to the central symmetry axis of the trap could be biased positively with respect to its opposite quadrant, creating a strong *radial* electric field in the same direction as the quadrupole radial electric field inside the trap, causing a magnetron drift which

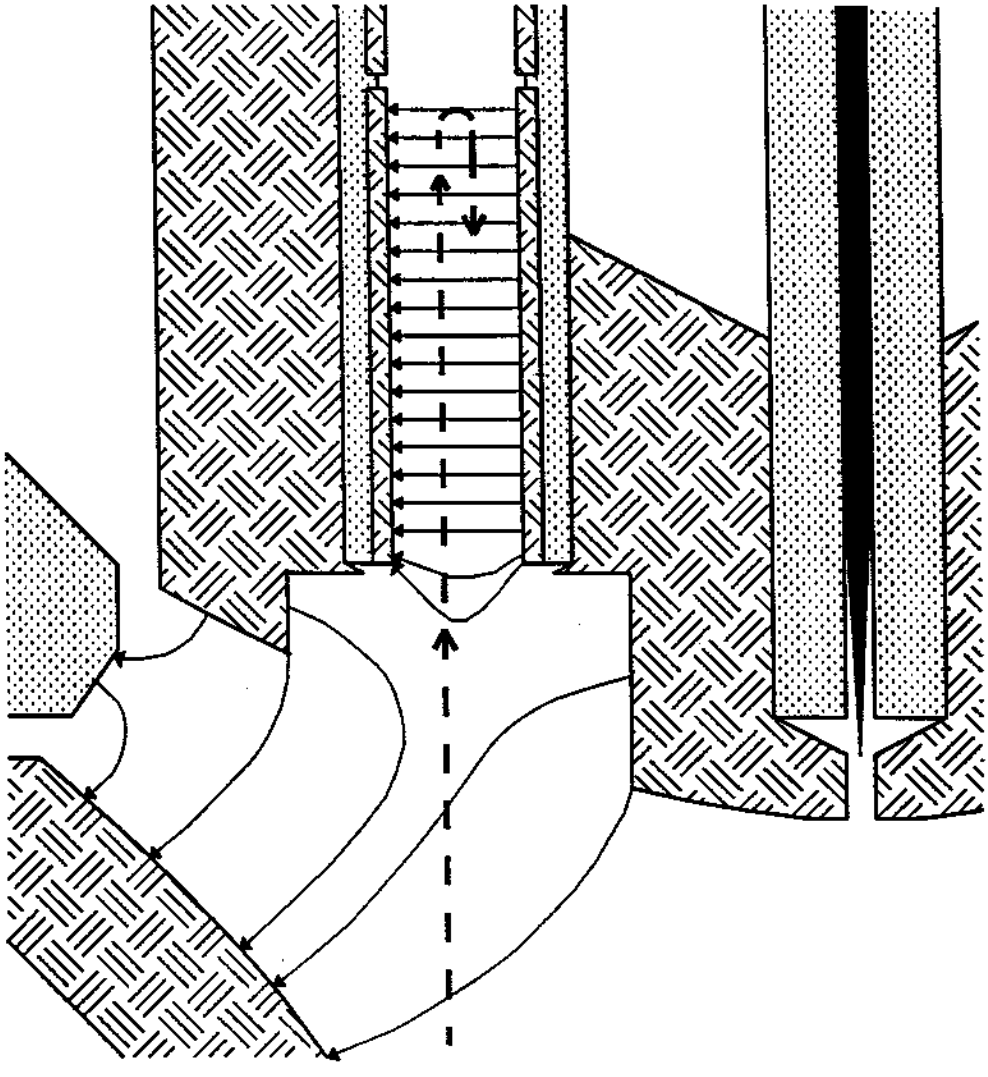

Figure 4.17: Proposed modification of the upper endcap aperture and upper entrance tube. Electric field lines are superimposed. The dashed line shows the trajectory of the positron. The upper tube is split into quadrants, allowing a strong radial electric field to be applied to increase $\delta_{\mathbf{mag}}$ locally.

is increased locally. The tube quadrants could be biased with a net negative potential (with respect to the endcaps) to insure that all moderated positrons would reach the upper tube interior; positrons could be prevented from leaking out the top end of the upper tube by adding a small, positively biased cylinder. The radial electric field inside the Penning trap during typical operating conditions is about 1 V/mm. The radial field inside the split upper tube could easily be about 1000 V/mm. This could virtually eliminate the factor of $(\delta_{\mathbf{mag}}/r_e)$ from Eq. 4.24, which would increase the loading rate R_L by a factor of ten or more. (To calculate this factor more precisely requires the solution to Laplace's equation in a split entrance tube, analogous to the calculations used in Section 4.2 for unsplit tubes. We have not yet undertaken this task.) It would be necessary to insure that positrons, having entered the (split) upper entrance tube and undergone magnetron drift, would be able to exit the tube and return to the trap volume. This could be done by grounding the remaining two tube quadrants and widening the entrance hole in the endcap electrode, as shown in Fig. 4.17. (The positrons' $\mathbf{E} \times \mathbf{B}$ motion would carry them towards a grounded tube segment, which they are energetically incapable of contacting.)

The modifications proposed in this section, along with the expected increases in R_L, are summarized in Table 4.1.

4.7 Useful electrons, unexpected positrons, and unwanted ions

There are a great many "free parameters" which must be set properly during the course of loading, accumulating, and detecting positrons. The radioactive source must be positioned so that positrons strike the moderator (Section 2.4). $V_{\mathbf{ring}}$, $V_{\mathbf{comp}}$, $V_{\mathbf{tube}}$, and $V_{\mathbf{mod}}$ must be set to accumulate positrons efficiently. After accumulating positrons for some time, $V_{\mathbf{ring}}$ and $V_{\mathbf{comp}}$ must be reset to allow

modification	parameter	current value	target value	expected gain
beam collimation	$\left(\frac{B_t}{B_s}\right)\left(\frac{r_e}{r_s}\right)$	$\sim .83$	1	1.2
magnetic "bounce"	$1-\sqrt{1-\left(\frac{B_s}{B_t}\right)}$	$\sim .17$	1	6
slow positron energy spread	ΔE	230 meV	$<$ 65 meV	3 to 4
moderator efficiency	η	1×10^{-4} (?)	10^{-3}	1 to 10
trapping voltage	$\sqrt[4]{V_0}$	$V_0 = 12$ V	1000 V	3
axial motion damping	$R = Q\omega L$	$Q = 750$	$Q = 1450$	2
magnetron drift distance	$\left(\frac{\delta_{\mathrm{mag}}}{r_e}\right)$	$\sim .02$	1	10 to 50
source activity	A	10 mCi	20 mCi	2

Table 4.1: Summary of proposed modifications to Penning trap which could increase in the positron loading rate.

for magnetron sideband cooling of the positrons, and the cooling drive strength. frequency, and sweep rate must be chosen to move positrons from their off-axis loading position to their on-axis detection position (Section 5.3). Fortunately, we were able to learn a great deal about most of these parameters by trapping electrons.

The on-axis field emission point mounted in the bottom endcap electrode (see Fig. 2.10) allows us to directly load electrons into the center of the trap, which in turn lets us test the detection and counting independently of how particles are loaded. The field emission point (FEP) emits a few nanoamps of current when it is

biased negatively by a few hundred volts. An electron beam current of 1 nA results in of order 10 electrons per second loaded into the center of the trap ($\rho \approx z \approx 0$), where they are detected and counted using their interaction with the damping circuit (Section 5.1). This technique is also used (at much lower electron beam currents) to load a single electron (or a very small number) into the center of the trap to measure the damping rate γ_z (Section 5.4).

Before we trapped any positrons, we perfected our magnetron cooling technique for moving particles from their off-axis loading position to the center of the trap ($\rho = 0$). We used the *off*-axis FEP to load (several hundred) electrons at $\rho = \rho_h$ and varied the magnetron cooling parameters until we found a technique which worked reliably. We later repeated this test with positrons (Section 5.3).

The dominant mechanism by which the FEP loads electrons into the trap is as follows: the energetic electron beam from the FEP (several hundred eV of energy) follows the magnetic field lines through the trap until it strikes a metal surface. The metal surface emits secondary electrons of about one percent of the primary beam. We measured that nearly all of these secondary electrons emerge with energies less than 3 eV. They return along the magnetic field lines, and some of them collide with the primary beam inside the trap volume. Some of these collisions result in electrons which transfer enough "axial" energy into cyclotron energy to be trapped. Once trapped, they rapidly cool to 4 K.

The measured loading rate of ~ 10 electrons per second from a 1 nA primary beam matches our expectations. Electrons emitted from the FEP with 500 eV energy have a range of cyclotron radii less than or equal to $r_c \approx 1.5 \times 10^{-3}$ cm and a velocity $v = 1.3 \times 10^9$ cm/sec. Because of the strong magnetic field, the electron beam area is $\sim \pi r_c^2$. Thus, the electron density in the (primary) beam at 1 nA (6.2×10^9 e^-/sec) is $n_{e^-} = 6.6 \times 10^5$ e^-/cm^3. Assuming a 1% emission efficiency of secondary electrons with 1 eV of energy, in a trap with length 1 cm, there is on average 1 secondary electron inside the trap volume at any given time when the primary beam is at 1 nA. Given a measured loading rate of $R = 10$ e^-/sec, the

calculated cross section for a trapping collision is $\sigma = R/vn_{e^-} = 1.1 \times 10^{-14}$ cm^2. This corresponds to an impact radius ($\sigma = \pi r_i^2$) of $r_i = 6 \times 10^{-8}$ cm. The Coulomb interaction energy between two charged particles at distance r_i is 2.4 eV, which is the expected order of magnitude for this process.

In the case of the off-axis FEP, the primary electron beam strikes is the moderator. When the moderator is biased positively ($V_{\rm mod} \geq +5$ Volts) or the bottom entrance tube is biased negatively ($V_{\rm tube} \leq -5$ Volts), the secondary electrons are energetically incapable of reaching the trap volume, and we detect no electrons (or very few) loaded into the trap. We know that it is possible to load positively charged ions into these traps via collisions between the primary electron beam and gas atoms released from the metal surfaces by the action of the electron beam. We would expect a few electrons to be loaded by this mechanism. The failure to detect trapped electrons when the moderator or tube are biased to prevent secondary electron return suggests that this mechanism is at least two orders of magnitude less efficient for this arrangement of electrodes.

The electron-electron collisional loading mechanism is quite different from the damping mechanism by which positrons are loaded into the trap. Electrons are loaded collisionally regardless of $V_{\rm ring}$ or $V_{\rm comp}$ (provided only that $V_{\rm ring}$ has the correct sign). Positrons are loaded via the damping mechanism only when the trap, tube, and moderator voltages are properly set within a fairly narrow region. Fortunately, we discovered that we could also trap (secondary) electrons via the damping mechanism by firing the off-axis FEP with the bottom entrance tube biased *positively* and the moderator biased positively by one or two volts. In fact, when $V_{\rm ring}$, $V_{\rm comp}$, $V_{\rm mod}$, and $V_{\rm tube}$ are adjusted to maximize the loading rate, a 10 pA (primary) beam results in of order 1000 electrons per second trapped, which is $\sim 10^4$ times more efficiently than the collisional mechanism. The success of this technique was our first verification that the damping mechanism would work for trapping positrons. The FEP provides a much more intense incident beam than the positron source, so that electrons can be accumulated and detected

far more quickly than positrons (and independent of the quality of the moderator preparation). This proved to be very useful in our initial studies of the damping mechanism.

The energetic positron beam from the radioactive source itself liberates slow secondary electrons from the moderator, with an efficiency much higher than η. (Several tens or hundreds of slow electrons per slow positron [48,49].) Moreover, these secondary electrons are emitted regardless of the quality of the moderator. We first trapped (via the damping mechanism) and detected these electrons a few weeks after discovering damped loading of secondary electrons produced by the FEP. It was our ability to load and detect these secondary electrons produced by the positron beam—when we were at first failing to trap positrons—which led us to replace our first, defective moderator.

A few positrons per hour load into our trap *regardless* of the values of V_{mod}, V_{tube}, or V_{ring}, provided that V_{ring} is negative and that the positron beam is traveling through the trap. Since the damping mechanism cannot be involved, we expect they load by some collisional process. We are not sure where these collisions are taking place. Positrons accumulate even when the resonant drives are applied which prevent ions from loading into the trap (see below), which suggests that collisions with trapped ions are not a factor. Positron impact with the sides of the entrance apertures is a possible source. Whatever the mechanism, the first positrons we ever trapped and detected were loaded in this way. (Positrons were loaded via the damping mechanism just a few weeks later, after we replaced the defective moderator.)

Unfortunately, positive ions also load into the trap during positron accumulation (or whenever the positron beam passes through the trap, provided the ring electrode is biased negatively). Trapped ions modify the otherwise harmonic axial motion of the positrons and prevent the trapped positrons from forming a "dip" in the noise spectrum of the LRC detection circuit (Section 5.1), which makes it

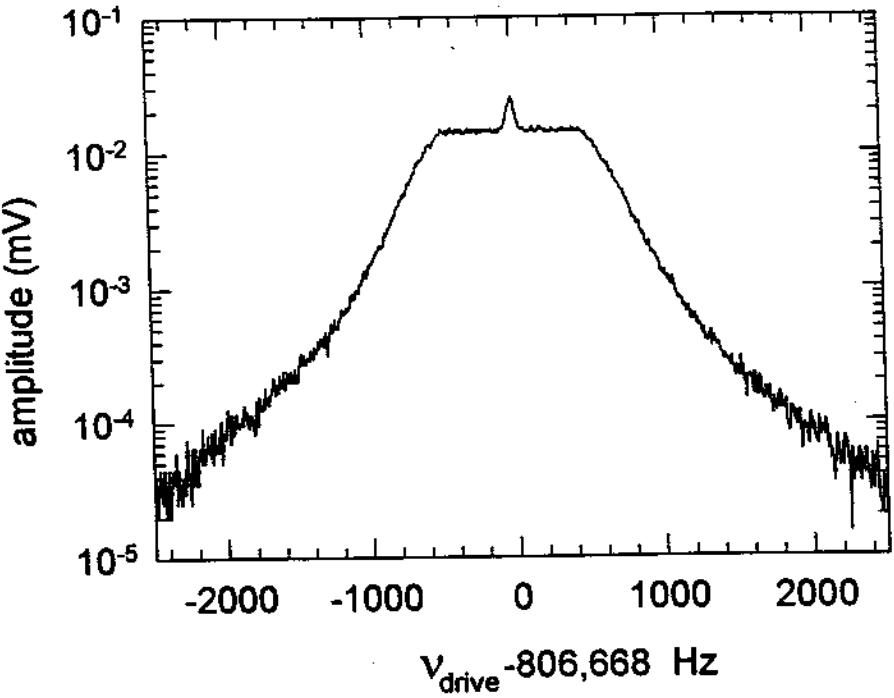

Figure 4.18: Frequency spectrum of the noise-broadened drive used to prevent ions from accumulating in the positron trap. The amplitude shown is applied to the magnet hat's vacuum feedthroughs, before losses in the transmission wires leading to the trap can. The drive frequency shown is for He^+. The axial frequency of other ions scales with the square root of the charge-to-mass ratio.

impossible to determine the number of positrons in the trap. It is still possible to *detect* the positrons via their response to the magnetron sideband excitation drive (Section 5.3), although far less effectively than when the trapped positrons are free from ions.

To prevent ions from loading during positron accumulation, we apply a drive to the bottom endcap electrode which is resonant with the axial frequencies of various ions. (The axial frequencies of the ions scale with the square root of their charge-to-mass ratio.) White noise derived from a frequency synthesizer (at +13 dBm power) is actively filtered (600 Hz low-pass), amplified (+20 dB), and mixed with the drive signal (at +7 dBm power) to noise-broaden the driving

frequency. Figure 4.18 shows a power spectrum of the resulting signal. The center frequency of the noise-broadened drive is swept in 100 Hz steps, 0.1 seconds per step, over a 1 kHz range around the axial frequency of each of the following ion species in succession: H^+, He^+, He^{++}, C^+, N^+, O^+, C_2^+, N_2^+, and O_2^+. This procedure appears to resonantly drive the ions out of the trap without affecting the positron loading. (The axial frequency of the positrons is much higher than that of the ions.) The ion drive is ***only*** applied during positron loading. While the positrons are being magnetron cooled and counted, we turn off the ion drive after closing the mechanical beam shutter.

During positron accumulation, electrons could potentially be trapped and accumulate in the region of the saddle potential at the bottom endcap aperture. A sufficiently large number of trapped electrons could shift V_{h0} due to space charge and thereby change the loading rate. To avoid this problem, we bias $V_{\mathbf{tube}}$ to +4 Volts and $V_{\mathbf{mod}}$ to +5 Volts for one second out of every minute of positron accumulation, which removes all electrons from the entrance tube region.